ACS APPLIED ENERGY MATERIALS

www.acsaem.org Article

MoS_2-Modified N-Doped Graphene/Organosulfide Composite Cathode Material for High-Performance Lithium–Sulfur Batteries

Yang Zhao, Zuhao Quan, Nuo Xu, Hongtao Zhang, and Yongsheng Chen*

Cite This: *ACS Appl. Energy Mater.* 2025, 8, 2360–2368 Read Online

ACCESS | Metrics & More | Article Recommendations | Supporting Information

ABSTRACT: Lithium–sulfur batteries (LSBs) possess merits of high theoretical specific capacity, high energy density, abundant resource, and low cost, making them promising candidates for future energy storage systems. Although numerous advanced high-performance LSBs have been studied, their further development still faces severe challenges. The redox intermediate lithium polysulfides (LiPSs) can be easily soluble in electrolytes and shuttles to anodes through a separator, leading to continuous loss of cathode-active materials and side reactions with lithium anodes, thereby compromising cycling stability. In addition, the sulfur cathode and its discharge product Li_2S exhibit poor electronic conductivity and undergo substantial volumetric changes during the discharge/charge process, affecting reaction kinetics and cycle life. To address these challenges, we developed an integrated system combining a MoS_2-modified N-doped graphene host material (MoS_2–NG) with an organosulfide-active material (S-SH), yielding a composite cathode material (MoS_2–NG@S-SH) with multiple advantages. The porous carbon-based MoS_2–NG host material, containing various heteroatoms, provides improved electronic conductivity, volume change buffering, physical barriers, chemical adsorption, and catalytic sites for LiPSs, synergistically suppressing the shuttle effect and facilitating the reaction kinetics. Furthermore, the S-SH active material features stable chemical bonds, contributing to enhanced cycling stability. Consequently, the MoS_2–NG@S-SH cathode delivers a high specific capacity of 1573.8 mA h g^{-1} at 0.05 C and maintains an exceptional average retention of 99.94% per cycle after 500 cycles at 1.0 C, demonstrating superior electrochemical performance.

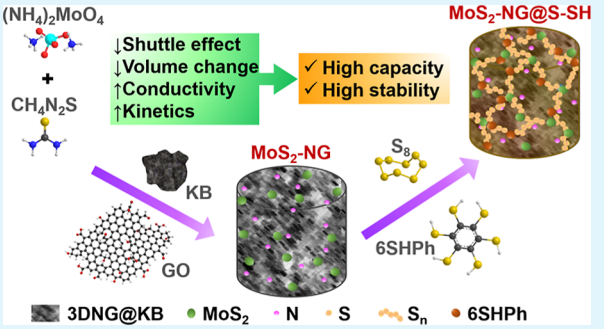

KEYWORDS: *energy storage, lithium–sulfur batteries, graphene-based host material, organosulfide material, high performance*

INTRODUCTION

The rapid global industrialization has led to unprecedented energy demands while simultaneously intensifying environmental concerns.[1,2] This dual challenge necessitates the development of both renewable energy sources and efficient energy storage systems (EESs).[3] Among various EESs, lithium-ion batteries (LIBs) have achieved widespread commercial success due to their merits of high energy density, lightweight construction, absence of memory effect, and extended cycle life.[4−7] However, conventional LIBs are approaching their theoretical limits in terms of specific capacity and energy density, creating a bottleneck for advancing electric vehicles and grid energy storage.[8] Lithium–sulfur batteries (LSBs), employing sulfur cathodes and lithium anodes, have emerged as a promising alternative to traditional LIBs, offering significantly higher theoretical capacity and energy density.[9−11] Furthermore, the transition from insertion-type cathodes to sulfur-based cathodes provides additional advantages, including the utilization of naturally abundant resource, cost-effectiveness, and environmental sustainability.[1,12]

In contrast to the intercalation mechanism in conventional LIBs, LSBs operate through a multiple-electron-transfer reaction (S_8 + 16 Li ↔ 8 Li_2S).[13,14] During the discharge process, S_8 undergoes sequential compositional and structural transformations (S_8 + 16 Li^+ + 16 e^- → 8 Li_2S), generating a series of intermediates lithium polysulfides (LiPSs) and Li_2S_2, forming the final product Li_2S. This conversion reaction contributes to the high theoretical specific capacity of 1672 mA h g^{-1}.[8,15,16] The reaction pathway is characterized by the formation of long-chain LiPSs (Li_2S_n, $2 < n \leq 8$), which are highly soluble in electrolytes, while the shorter-chain species Li_2S_2 and the discharge product Li_2S remain insoluble.[14] At the anode, lithium undergoes oxidation during the discharge process (Li–e^- → Li^+), delivering a high theoretical capacity of 3860 mA h g^{-1}.[10] The LSB system operates at an average working potential of ∼2.1 V, resulting in a high theoretical energy density of ∼2600 Wh kg^{-1}.[10]

Received: November 18, 2024
Revised: February 8, 2025
Accepted: February 10, 2025
Published: February 13, 2025

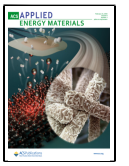

https://doi.org/10.1021/acsaem.4c02954
ACS Appl. Energy Mater. 2025, 8, 2360–2368

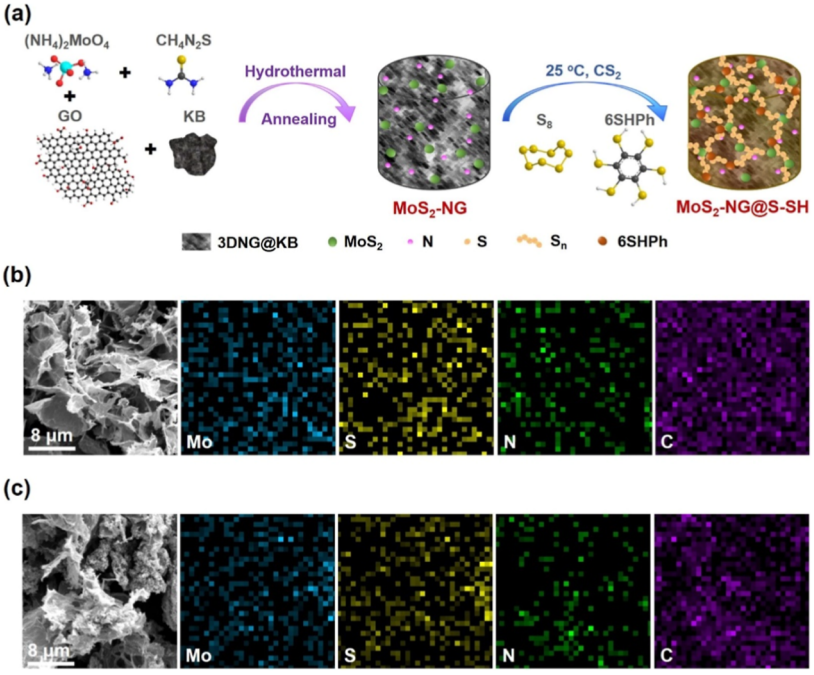

Figure 1. Preparation and characterizations of the MoS_2−NG host material and MoS_2−NG@S-SH composite material. (a) Schematic diagram for the preparation processes of MoS_2−NG and MoS_2−NG@S-SH materials. Scanning electron microscope (SEM) and energy-dispersive spectrometer (EDS) images for (b) MoS_2−NG host material and (c) MoS_2−NG@S-SH composite material.

Many advanced LSBs have demonstrated superior electrochemical performance; however, several major obstacles impede their further development and large-scale commercialization.[17−20] One major issue is the polysulfide shuttle effect, where highly soluble LiPS intermediates diffuse from the cathode to the anode through the electrolyte and separator. This phenomenon leads to a continuous loss of cathode-active materials and serious side reactions with the lithium anode, resulting in severe self-discharge and poor cycling stability.[10,12,21−23] Additionally, there is a notable density difference between the sulfur cathode (2.07 g cm^{-3}) and its discharge product Li_2S (1.66 g cm^{-3}). This discrepancy causes significant volumetric variation (~80%) and structural damage during the electrochemical process, contributing to the capacity fade and reduced cycle life.[24,25] Furthermore, both solid-state sulfur and Li_2S suffer from poor electronic conductivity, leading to sluggish reaction kinetics and inferior electrochemical performance.[25]

To address the challenges of LSBs, extensive studies have been conducted on various strategies. These strategies primarily involve physical barriers, chemical adsorption, and chemical bonds to suppress the shuttle effect of LiPSs.[21] Two-dimensional or porous carbon-based materials, such as graphene, carbon nanotubes, and carbon nanofibers, serve as effective physical barriers that enhance cycling performance.[1,21] Additionally, porous carbon-based materials also enhance electronic conductivity and ameliorate volumetric variation during the discharge/charge process, thereby improving reaction kinetics and cycling stability.[26,27] Chemical approaches include the use of polar host materials, such as metallic oxides/sulfides, heteroatom-doped carbon materials, and metal−organic frameworks. These materials can chemically adsorb LiPSs through polar−polar interactions, effectively suppressing LiPS dissolution.[21,28] Furthermore, organosulfide materials possess stable chemical bonds between LiPSs and organic molecules, which help mitigate volumetric changes and material pulverization, thus synergistically improving cycling performance.[9,29] Another significant advancement involves the catalytic conversion between LiPSs and Li_2S_2/Li_2S. This process, facilitated by transitional metal compounds, metals, or metal-free materials, not only accelerates reaction kinetics but also suppresses the shuttle effect, leading to improved sulfur utilization and electrochemical performance.[10,30]

Based on these considerations, the combination of heteroatom-doped (such as S, N, and O) porous carbon-based materials, catalytically active transitional metal compounds (such as metal oxides, sulfides, and nitrides), and stable organosulfides can achieve synergistic effects in suppressing the LiPS shuttle effect, improving electronic conductivity, enhancing reaction kinetics, and buffering volumetric changes.[24,31] In this work, we design and prepare a composite cathode material (MoS_2−NG@S-SH) by in situ integrating a MoS_2-modified N-doped graphene host material (MoS_2−NG) and an organosulfide-active material (S-SH) to achieve high electrochemical performance in LSBs. The MoS_2−NG host material is fabricated through a one-step hydrothermal method, followed by annealing, using precursors of ammonium molybdate ($(NH_4)_2MoO_4$), thiourea (CH_4N_2S), graphene oxide (GO), and Ketjen Black (KB).[28,32−34] The MoS_2−NG@S-SH composite material is subsequently synthesized by in situ cross-linking of sulfur (S_8) with benzenehexathiol (6SHPh) on the MoS_2−NG host material.[35,36] Therefore, the MoS_2−NG@S-SH composite cathode material incorporates physical barriers, chemical adsorption sites, chemical bonds, and rapid catalytic reaction ability, effectively suppressing the LiPS shuttle effect and improving reaction kinetics. Additionally, the MoS_2−NG@S-SH cathode material possesses enhanced conductivity and reduced volumetric changes, contributing to excellent electrochemical performance. As a result, the MoS_2−NG@S-SH cathode delivers a high specific capacity of 1573.8

https://doi.org/10.1021/acsaem.4c02954
ACS Appl. Energy Mater. 2025, 8, 2360−2368

mA h g^{-1} at 0.05 C (83.6 mA g^{-1}), exhibiting a high specific capacity and high utilization of sulfur. It also demonstrates an average capacity retention of 99.94% per cycle for 500 cycles at 1.0 C (1672 mA g^{-1}), indicating remarkable cycling stability. These results reveal that our strategy of combining the MoS_2-modified N-doped graphene host material with the organosulfide-active material provides synergistic effects and significantly enhances the electrochemical performance of LSBs, showing promise for future LSB and EES applications.

RESULTS AND DISCUSSION

The MoS_2−NG host material was prepared through a one-step solvothermal method using ammonium molybdate ($(NH_4)_2MoO_4$), thiourea (CH_4N_2S), graphene oxide (GO), and Ketjen Black (KB) as precursors. After the mixture was heated at 180 °C for 24 h and annealed at 300 °C for 4 h under argon, a MoS_2-modified three-dimensional N-doped graphene-KB network (3DNG@KB) was constructed, yielding the MoS_2−NG host material (Figure 1a).

The MoS_2−NG host material was subsequently mixed with sulfur (S_8) and benzenehexathiol (6SHPh) in a CS_2 solvent, and the mixture was stirred under 25 °C for 24 h. During this process, S_n ($0 < n < 8$) chemically cross-linked with 6SHPh to form organosulfide S-SH (Figure S1),[36] simultaneously producing the MoS_2−NG@S-SH composite material. The MoS_2−NG host material exhibits a characteristic porous morphology with uniform elemental distribution of Mo, S, N, and C (Figures 1b, S2, and S3). After in situ loading with the S-SH active material, the pores of the MoS_2−NG network were partly filled, showing uniform elemental distribution throughout the MoS_2−NG@S-SH composite material (Figures 1c and S4).

The MoS_2−NG host material exhibits a large Brunauer−Emmett−Teller (BET) surface area of 402.62 m^2 g^{-1}, which can be attributed to the porosity of the graphene-KB network (Figure 2a). After in situ loading with organosulfide S-SH, the BET surface area of the MoS_2−NG@S-SH composite material reduced to 60.23 m^2 g^{-1}, indicating partly filled pores for the MoS_2−NG host material by the S-SH active material, which is consistent with the results of SEM images. Each 6SHPh molecule contains six thiol groups (-SH), which could react with S_8 in CS_2 at 25 °C to form the organosulfide S-SH (Figure S1). The FT-IR spectrum of 6SHPh reveals a characteristic peak of −SH at 2505.1 cm^{-1}[36] (Figure 2b). In the FT-IR spectrum of the MoS_2−NG@S-SH composite material, the −SH peak nearly disappears, while a new peak corresponding to S−S bonds emerges at 467.7 cm^{-1},[11,37] revealing the consumption of −SH groups from the 6SHPh cross-linker and the formation of organosulfide with multiple S−S bonds (Figure 2b). The Raman spectra of MoS_2−NG and MoS_2−NG@S-SH materials demonstrate characteristic D and G peaks of the carbon-based graphene-KB network (Figure 2c).[38]

The XPS survey spectrum of MoS_2−NG (Figure S5) and MoS_2−NG@S-SH (Figure 2d) shows characteristic peaks of S 2p, Mo 3d, C 1s, N 1s, Mo 3p, and O 1s,[39,40] confirming their elemental compositions. The XPS survey spectra of MoS_2−NG@S-SH exhibits an intensified peak of S 2p, indicating increased sulfur content and successful incorporation of organosulfide S-SH. The high-resolution XPS C 1s spectrum for the MoS_2−NG host material in Figure S6a displays characteristic peaks at 284.6 (C−Mo), 285.0 (C−C and C═C), 286.1 (C−S), 288.9 (C−O and C−N), and 292.0 eV ($\pi-\pi^*$).[11,41−43] These peaks shift to lower binding energy in

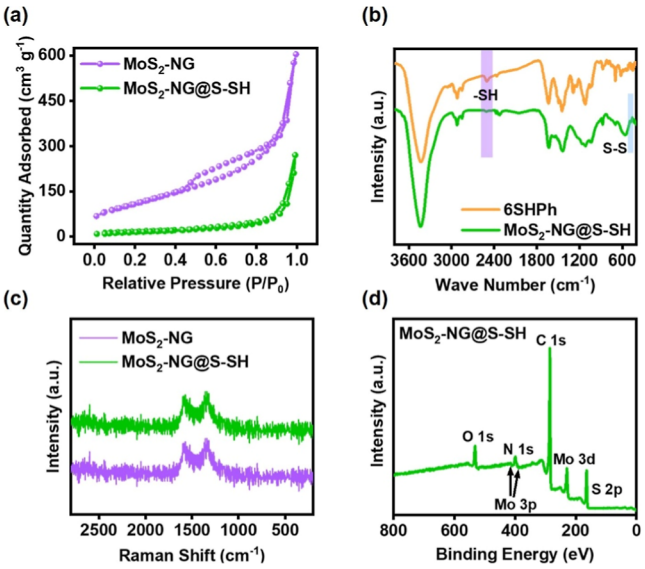

Figure 2. Material characterizations of the MoS_2−NG host material and MoS_2−NG@S-SH composite material. (a) Brunauer−Emmett−Teller (BET) isotherms for MoS_2−NG and MoS_2−NG@S-SH materials under 77 K. (b) Fourier transform infrared (FT-IR) spectra for 6SHPh and MoS_2−NG@S-SH materials. (c) Raman spectra for MoS_2−NG and MoS_2−NG@S-SH materials. (d) X-ray photoelectron spectroscopy (XPS) for MoS_2−NG@S-SH materials.

the C 1s spectrum of the MoS_2−NG@S-SH material after loading organosulfide S-SH (Figure S6b), indicating the interaction between the carbon-based host material and S-SH-active material.[32] The XPS S 2p spectrum for the MoS_2−NG@S-SH composite material displays peaks of S−Mo (162.4 eV), S−S and S−C (164.4 and 165.6 eV), and S−O and S═O (168.7 eV), and it exhibits enhanced S−S and S−C peaks than that of MoS_2−NG, confirming the successful integration of organosulfide S-SH with the MoS_2−NG host material (Figure S7). The XPS Mo 3d spectrum of MoS_2−NG in Figure S8a shows the characteristic peaks of Mo−S (229.8/233.5 eV), Mo−C (229.4/232.7 eV), and Mo−N (231.0/235.7 eV).[40,41,44,45] In the Mo 3d XPS spectrum of the MoS_2−NG@S-SH composite material, the Mo−S peaks intensify and shift to lower binding energy (229.5/233.4 eV), indicating the incorporation of organosulfide S-SH and its interaction with Mo (Figure S8b). Additionally, the Mo−C and Mo−N peaks also shift to lower binding energy at 228.4/232.6 and 230.7/235.5 eV, respectively. The negative shifts observed in both XPS C 1s and Mo 3d spectra for MoS_2−NG@S-SH can be attributed to the increased electron density around C and Mo atoms, suggesting that electrons transfer from S atoms in the S-SH active material to Mo and C atoms in the MoS_2−NG host material, thus confirming the interaction between MoS_2−NG and S-SH.[32,40]

Thermogravimetric analysis (TGA) conducted under N_2 for the MoS_2−NG host material demonstrates a negligible mass loss of 2.72% over 300 °C, suggesting its thermal stability. Additionally, it could be calculated that the S-SH active material loading exceeds 50 wt % in the MoS_2−NG@S-SH composite material (Figure S9). Elemental analysis shows that Mo and S contents are 4.11 and 56.98 wt %, respectively, in the MoS_2−NG@S-SH composite material (Table S1). The calculated active S loading of 54.24 wt % corroborates the TGA results. The X-ray diffraction (XRD) pattern of the

https://doi.org/10.1021/acsaem.4c02954
ACS Appl. Energy Mater. 2025, 8, 2360−2368

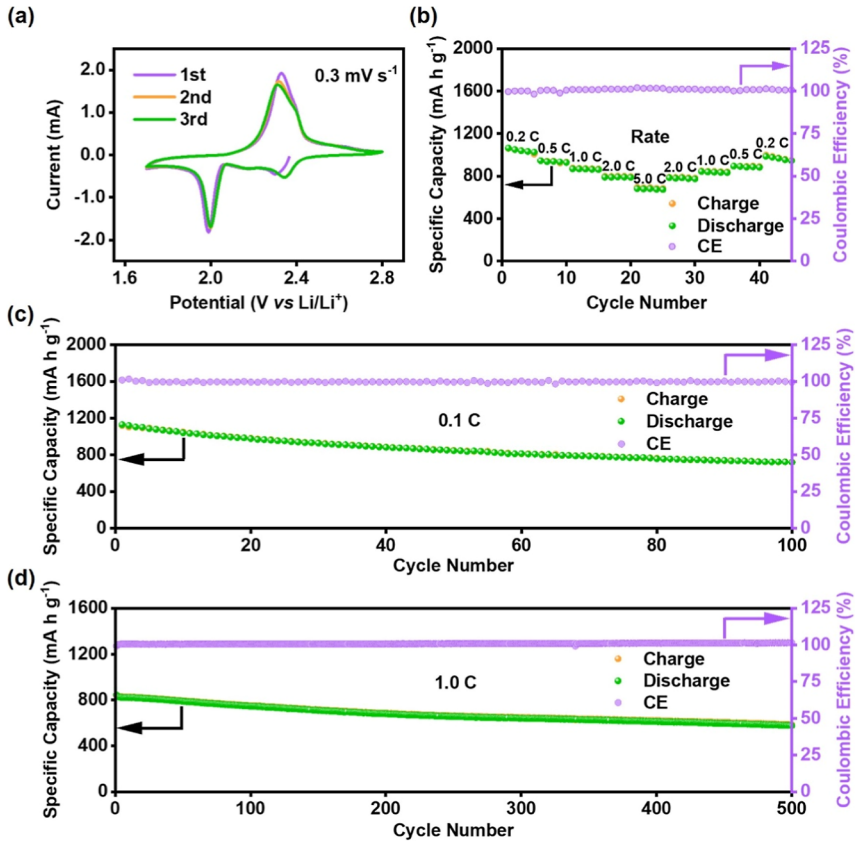

Figure 3. Electrochemical performance of the MoS_2−NG@S-SH cathode. (a) Cyclic voltammetry (CV) curves for the MoS_2−NG@S-SH cathode. (b) Rate performance for the MoS_2−NG@S-SH cathode at 0.2, 0.5, 1.0, 2.0, and 5.0 C, respectively. (c) Cycling performance for the MoS_2−NG@S-SH cathode under 0.1 C for 100 cycles. (d) Cycling performance for the MoS_2−NG@S-SH cathode at 1.0 C for 500 cycles.

MoS_2−NG host material in Figure S10 exhibits weak diffraction peaks corresponding to the (002), (101), and (110) planes of MoS_2, indicating its low crystallinity.[46−49] Additionally, characteristic graphene peaks of (002) and (110) are observed.[48]

The MoS_2−NG@S-SH composite material was evaluated as a cathode-active material for LSBs, within an electrochemical window of 1.7−2.8 V (vs Li/Li^+). The redox process for the S-SH active material in the MoS_2−NG@S-SH cathode is illustrated in Figure S11.[36,50,51] When discharged, S-SH could be partly reduced, generating lithium polysulfides, which could transform to $C_6S_6Li_6$ and Li_2S with further reduction. Cyclic voltammetry (CV) curves of the MoS_2−NG@S-SH cathode at 0.3 mV s^{-1} (~1.0 C) are presented in Figure 3a, showing characteristics similar to those of the S electrode (Figure S15a). The cathodic peaks at 2.34 V (vs Li/Li^+) can be attributed to the transformation of LiPSs, while the peak at 2.00 V (vs Li/Li^+) represents the subsequent formation of lithium sulfide (Li_2S).[50,51] An overlapped anodic peak is observed at approximately 2.31 V (vs Li/Li^+), corresponding to the reversible oxidation of Li_2S and formation of LiPSs.[36,50,51] The initial three cycles of CV curves display minimal deviation, indicating excellent redox reversibility of the MoS_2−NG@S-SH cathode.

The MoS_2−NG@S-SH cathode demonstrates remarkable electrochemical performance, exhibiting a high specific capacity of 1573.8 mA h g^{-1} at 0.05 C (83.6 mA g^{-1}), which corresponds to an impressive capacity utilization of 94.1% (Figure S12). The redox potential plateaus of this cathode align well with the redox peaks observed in the CV curves. When tested at various rates, the MoS_2−NG@S-SH cathode delivers specific capacities of 1064.7, 944.6, 866.5, 789.4, and 681.1 mA h g^{-1} at rates of 0.2, 0.5, 1.0, 2.0, and 5.0 C, respectively. When returning to lower rates, the capacity could recover to the initial high values, surpassing the typical S cathode (Figures 3b, S13, and S15b). In cycling measurements, the MoS_2−NG@S-SH cathode shows an initial specific capacity of 1120.1 mA h g^{-1} at 0.1 C (167.2 mA g^{-1}) and maintains a near-100% Coulombic efficiency throughout 100 cycles (Figure 3c). When cycled at 1.0 C (1672 mA g^{-1}), it maintains a high discharge capacity of ~600 mA h g^{-1} after 500 cycles, exhibiting an average capacity retention of 99.94% per cycle (Figure 3d). The MoS_2−NG@S-SH cathode is further validated at both 0.5 (836 mA g^{-1}) and 2.0 C (3344 mA g^{-1}), indicating effective suppression of the LiPS shuttle effect and enhanced stability (Figure S14). Comprehensive testing across all rates consistently demonstrates that the MoS_2−NG@S-SH cathode outperforms conventional S cathodes in both specific capacity and cycling stability (Figure S15).

GITT analysis was conducted on both MoS_2−NG@S-SH and S cathodes (Figures 4a,b, S16a, and S16b). During the Li_2S nucleation process, MoS_2−NG@S-SH and S cathodes deliver potential drops (ΔiR) of 21.7 and 109.4 mV, respectively. For Li_2S activation, the ΔiR values were 491.3 and 793.3 mV for MoS_2−NG@S-SH and S cathodes, respectively.[52,53] The MoS_2−NG@S-SH cathode exhibits lower voltage differences (ΔiR) for both Li_2S nucleation and activation processes compared to the S cathode, suggesting the

https://doi.org/10.1021/acsaem.4c02954
ACS Appl. Energy Mater. 2025, 8, 2360−2368

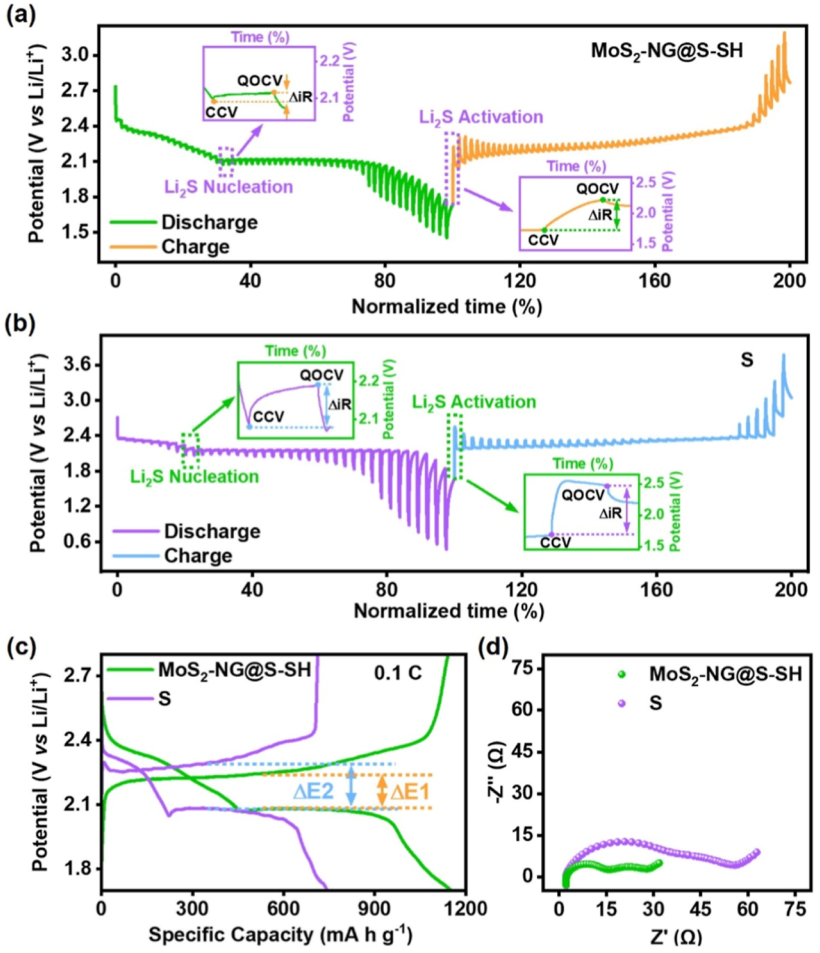

Figure 4. Kinetics analysis for MoS_2−NG@S-SH and S cathodes. Galvanostatic intermittent titration technique (GITT) for (a) MoS_2−NG@S-SH cathode and (b) S cathode. (c) Galvanostatic charge−discharge profiles for MoS_2−NG@S-SH and S cathodes. (d) Electrochemical impedance spectroscopy (EIS) for MoS_2−NG@S-SH and S cathodes.

alleviated polarization and redox kinetic limitations (Figure 4a,b).[52,53]

The lithium-ion diffusion coefficients (D) were calculated from the GITT results (Figure S16c).[54] The MoS_2−NG@S-SH cathode shows higher D than that of the S cathode during the discharge/charge process, indicating enhanced Li-ion diffusion and better kinetics. Additionally, CV curves at different scan rates were measured to further study the diffusion coefficients (D) of MoS_2−NG@S-SH and S cathodes (Figure S17a and S17b). The D could be obtained through the slope for plots of I_p^2 against v, where I_p is the peak current and v represents different scan rates (Figure S17c and S17d). The MoS_2−NG@S-SH cathode shows a higher D value compared to that of the S cathode during the cathodic and anodic processes, indicating faster kinetics, which is consistent with the GITT results.

The internal resistance ($\Delta R_{internal}$) related to the discharge/charge process can be indicated from the dip depth in the galvanostatic charge/discharge profiles.[53] The internal resistance is calculated using the equation: $\Delta R_{internal}$ (Ω) = $|\Delta V_{QOCV\text{-}CCV}|/i$, where "$\Delta V$" is the voltage difference between the quasi-open circuit voltage (QOCV) and the closed circuit voltage (CCV) and "i" is the applied current.[55] The relative internal resistances of S and MoS_2−NG@S-SH cathodes were plotted against normalized capacity for the discharge/charge process. The analysis reveals that the MoS_2−NG@S-SH cathode displays consistently lower relative internal resistance compared to the S cathode throughout the electrochemical process (Figure S16d).[41,56−58]

The polarization potential (ΔE) obtained from galvanostatic charge−discharge profiles reveals the hysteresis in the redox reaction.[59] The S cathode possesses a polarization potential ($\Delta E2$) of 211.4 mV at 0.1 C, while the MoS_2−NG@S-SH cathode exhibits a narrower polarization potential ($\Delta E1$) of 165.3 mV, revealing enhanced sulfur reaction kinetics (Figure 4c).[17] EIS analysis was conducted on both MoS_2−NG@S-SH and S cathodes, revealing that the MoS_2−NG@S-SH cathode exhibits significantly lower charge-transfer resistance compared to the S cathode (Figure 4d), which is consistence with the GITT results. The combination of a higher lithium-ion diffusion coefficient, lower polarization potential, and reduced resistance demonstrates enhanced redox kinetics for the MoS_2−NG@S-SH cathode, contributing to its superior electrochemical performance.

The suppression of the shuttle effect on LPSs was also studied. The LSB using the MoS_2−NG@S-SH cathode possess a cleaner separator and a flatter lithium anode under SEM than that of the S cathode, indicating a reduction in the shuttle effect of LPSs and mitigated corrosion of the lithium anode (Figure S18). Additionally, a Li_2S_6 solution was prepared and treated with the MoS_2−NG host material (Li_2S_6+MoS_2−NG). The color of the Li_2S_6+MoS_2−NG solution is lighter, along

https://doi.org/10.1021/acsaem.4c02954
ACS Appl. Energy Mater. 2025, 8, 2360−2368

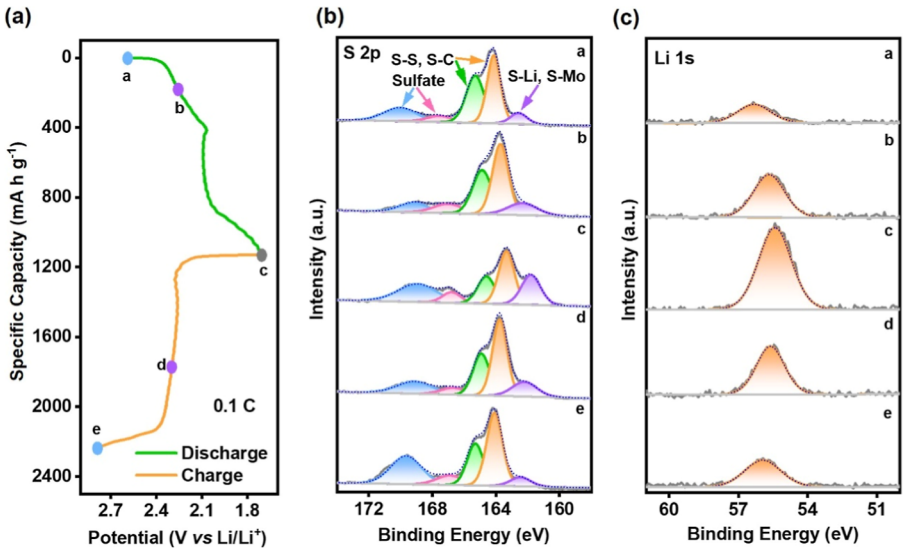

Figure 5. Redox process analysis for the MoS_2−NG@S-SH cathode. (a) Galvanostatic charge−discharge profiles and different potential states for the MoS_2−NG@S-SH cathode. (b) Ex situ XPS S 2p spectra for the MoS_2−NG@S-SH cathode at different potential states. (c) Ex situ XPS Li 1s spectra for the MoS_2−NG@S-SH cathode at different potential states.

with the decreased UV−vis absorption than that of Li_2S_6 solution, suggesting the depressed shuttle effect of LPSs (Figure S19).

Additionally, we fabricated LSBs using MoS_2−NG@S-SH and S cathodes with a high mass loading. The MoS_2−NG@S-SH cathode with a mass loading of 5.0 mg cm^{-2} displays capacities of 652.1, 548.2, 509.3, and 354.5 mA h g^{-1} at rates of 0.2, 0.5, 1.0, and 2.0 C, respectively (Figure S20b), which is better than that of the S cathode with a mass loading of 2.8 mg cm^{-2} (Figure S20a). High initial capacities of 994.0 and 603 mA h g^{-1} could be obtained for the MoS_2−NG@S-SH cathode under 0.1 C with a mass loading of 5.5 mg cm^{-2} and under 0.5 C with a mass loading of 7.0 mg cm^{-2}, respectively, which also shows high stability (Figures S20c and S20d). The MoS_2−NG@S-SH cathode exhibits higher capacity, improved cycle stability, and superior rate performance compared to the S cathode, demonstrating better overall electrochemical performance.

To study the redox reaction process of the MoS_2−NG@S-SH cathode, *ex situ* XPS analysis was conducted on it at different potential states (Figure 5). State "a" represents the pristine electrode after immersing in an electrolyte at an open current voltage. States "b" and "c" represent the electrodes discharged to 2.3 and 1.7 V (vs Li/Li^+), respectively. When charged to 2.3 and 2.8 V (vs Li/Li^+), the electrodes are marked as state "d' and "e", respectively (Figure 5a). Figure 5b displays high-resolution XPS S 2p spectra for the five different states of the MoS_2−NG@S-SH cathode during the redox process. In the initial state (state "a"), the MoS_2−NG@S-SH cathode exhibits a peak at 162.6 eV corresponding to S−Li and S−Mo, which can be attributed to the Li^+ adsorption from the electrolyte.[40,60,61] The S−S and S−C bonds of polysulfide appear at 164.2/165.3 eV, respectively, while sulfate peaks are observed at 167.6 and 170.1 eV, originating from $TFSI^-$ in the electrolyte.[51,60−63] When further discharged to 1.7 V (*vs Li/Li*$^+$) (state "c"), the peak of S−Li negatively shifts to 161.9 eV, while the peaks of S−S and S−C also negatively shift to 163.3/164.6 eV. During the successive discharge process (state "b" and "c"), the XPS S 2p spectra gradually shift to lower binding energy, accompanied by the decreased peak of S−S and the increased peak of S−Li. These observations indicate the increase in electrons density around S atoms, reduction of S−S bonds, and formation of S−Li interactions in the MoS_2−NG@S-SH cathode during the discharge process.[32,40,61,64] Throughout the charge process (state "d" and "e"), the XPS S 2p spectra gradually recover to their initial states, revealing good redox reversibility of the MoS_2−NG@S-SH cathode.[64] Ex situ XPS Li 1s spectra of the MoS_2−NG@S-SH cathode also exhibit reversible changes during the discharge/charge process (Figure 5c). The Li 1s peak increases when discharge and decreases when charge, suggesting the combination/dissociation of Li ions during the discharge/charge process, which corresponds to the reversible changes of the S 2p spectra observed in the electrochemical process.[63,65,66]

CONCLUSIONS

In conclusion, we have successfully designed and prepared a MoS_2−NG@S-SH composite cathode material that demonstrates an exceptional performance in LSBs. The innovative design incorporates a MoS_2-modified N-doped graphene-KB host material, which endows MoS_2−NG@S-SH with effective physical barriers, chemical adsorption sites, alleviative volumetric changes, enhanced conductivity, and improved reaction kinetics. These combined features contribute significantly to the material's high specific capacity and remarkable cycling stability. The integration of the organosulfide active material further improves cycling stability. As a result, the MoS_2−NG@S-SH cathode exhibits an impressive specific capacity of 1573.8 mA h g^{-1} at 0.05 C, revealing high sulfur utilization. Furthermore, the cathode delivers excellent cycling performance at different current densities, as well as remarkable rate performance. These results demonstrate that the MoS_2−NG@S-SH composite material shows superior electrochemical performance, validating our synergistic design strategy as an effective approach for developing advanced LSBs in the future.

https://doi.org/10.1021/acsaem.4c02954
ACS Appl. Energy Mater. 2025, 8, 2360−2368

■ ASSOCIATED CONTENT

Supporting Information

The Supporting Information is available free of charge at https://pubs.acs.org/doi/10.1021/acsaem.4c02954.

Reagents and materials; instruments and characterizations; preparation of GO, MoS_2-NG, S-SH, and MoS_2-NG@S-SH; cell preparations and electrochemical characterizations; synthesis route and chemical structure; SEM images; XPS; high-resolution XPS C 1s spectra; high-resolution XPS S 2p spectra; high-resolution XPS Mo 3d spectra; TGA results; XRD; redox process; capacity−voltage profiles; cycle performance; electrochemical performance; kinetics analysis; CV curves; suppression for the shuttle effect; UV−vis absorption spectra; electrochemical performance; and elemental analysis (PDF)

■ AUTHOR INFORMATION

Corresponding Author

Yongsheng Chen − *The Centre of Nanoscale Science and Technology and Key Laboratory of Functional Polymer Materials, Institute of Polymer Chemistry, College of Chemistry, Nankai University, Tianjin 300071, China; State Key Laboratory of Elemento-Organic Chemistry and Renewable Energy Conversion and Storage Center (RECAST), Nankai University, Tianjin 300071, China;* orcid.org/0000-0003-1448-8177; Email: yschen99@nankai.edu.cn

Authors

Yang Zhao − *The Centre of Nanoscale Science and Technology and Key Laboratory of Functional Polymer Materials, Institute of Polymer Chemistry, College of Chemistry, Nankai University, Tianjin 300071, China; Renewable Energy Conversion and Storage Center (RECAST), Nankai University, Tianjin 300071, China; SINOPEC (Beijing) Research Institute of Chemical Industry Co., Ltd., Beijing 100013, China*

Zuhao Quan − *The Centre of Nanoscale Science and Technology and Key Laboratory of Functional Polymer Materials, Institute of Polymer Chemistry, College of Chemistry, Nankai University, Tianjin 300071, China; Renewable Energy Conversion and Storage Center (RECAST), Nankai University, Tianjin 300071, China*

Nuo Xu − *The Centre of Nanoscale Science and Technology and Key Laboratory of Functional Polymer Materials, Institute of Polymer Chemistry, College of Chemistry, Nankai University, Tianjin 300071, China; Renewable Energy Conversion and Storage Center (RECAST), Nankai University, Tianjin 300071, China*

Hongtao Zhang − *The Centre of Nanoscale Science and Technology and Key Laboratory of Functional Polymer Materials, Institute of Polymer Chemistry, College of Chemistry, Nankai University, Tianjin 300071, China; Renewable Energy Conversion and Storage Center (RECAST), Nankai University, Tianjin 300071, China*

Complete contact information is available at: https://pubs.acs.org/10.1021/acsaem.4c02954

Notes

The authors declare no competing financial interest.

■ ACKNOWLEDGMENTS

The authors gratefully acknowledge the financial support from the National Natural Science Foundation of China (NSFC, 52090034) and the Ministry of Science and Technology of China (MoST, 2020YFA0711500).

■ REFERENCES

(1) Manthiram, A.; Fu, Y.; Su, Y.-S. Challenges and Prospects of Lithium-Sulfur Batteries. *Acc. Chem. Res.* **2013**, *46* (5), 1125−1134.

(2) Sun, J.; Xu, Y.; Lv, Y.; Zhang, Q.; Zhou, X. Recent Advances in Covalent Organic Framework Electrode Materials for Alkali Metal-Ion Batteries. *CCS Chem.* **2023**, *5* (6), 1259−1276.

(3) Manthiram, A.; Chung, S.-H.; Zu, C. Lithium-Sulfur Batteries: Progress and Prospects. *Adv. Mater.* **2015**, *27* (12), 1980−2006.

(4) Evers, S.; Nazar, L. F. New Approaches for High Energy Density Lithium-Sulfur Battery Cathodes. *Acc. Chem. Res.* **2013**, *46* (5), 1135−1143.

(5) Chung, S.-H.; Manthiram, A. Current Status and Future Prospects of Metal-Sulfur Batteries. *Adv. Mater.* **2019**, *31* (27), 1901125.

(6) Huang, W.; Zhang, X.; Zheng, S.; Zhou, W.; Xie, J.; Yang, Z.; Zhang, Q. Calix[6]Quinone as High-Performance Cathode for Lithium-Ion Battery. *Sci. China Mater.* **2020**, *63* (3), 339−346.

(7) Dong, Q.; Naren, T.; Zhang, L.; Jiang, W.; Xue, M.; Wang, X.; Chen, L.; Lee, C.-S.; Zhang, Q. A Naphthalenetetracarboxdiimide-Containing Covalent Organic Polymer: Preparation, Single Crystal Structure and Battery Application. *Angew. Chem., Int. Ed.* **2024**, *63* (26), No. e202405426.

(8) Hu, A.; Zhou, M.; Lei, T.; Hu, Y.; Du, X.; Gong, C.; Shu, C.; Long, J.; Zhu, J.; Chen, W.; Wang, X.; Xiong, J. Optimizing Redox Reactions in Aprotic Lithium-Sulfur Batteries. *Adv. Energy Mater.* **2020**, *10* (42), 2002180.

(9) Wang, D.-Y.; Guo, W.; Fu, Y. Organosulfides: An Emerging Class of Cathode Materials for Rechargeable Lithium Batteries. *Acc. Chem. Res.* **2019**, *52* (8), 2290−2300.

(10) Lim, W.-G.; Kim, S.; Jo, C.; Lee, J. A Comprehensive Review of Materials with Catalytic Effects in Li-S Batteries: Enhanced Redox Kinetics. *Angew. Chem., Int. Ed.* **2019**, *58* (52), 18746−18757.

(11) Wang, Y.; Luo, Z.; Zhou, J.; Fan, X.; Zhang, J.; Jia, Y.; Chen, S.; Meng, X.; Bielawski, C. W.; Geng, J. Covalently Grafting Sulfur-Containing Polymers to Carbon Nanotubes Enhances the Electrochemical Performance of Sulfur Cathodes. *ACS Appl. Polym. Mater.* **2022**, *4* (2), 939−949.

(12) Zhou, J.; Holekevi Chandrappa, M. L.; Tan, S.; Wang, S.; Wu, C.; Nguyen, H.; Wang, C.; Liu, H.; Yu, S.; Miller, Q. R. S.; Hyun, G.; Holoubek, J.; Hong, J.; Xiao, Y.; Soulen, C.; Fan, Z.; Fullerton, E. E.; Brooks, C. J.; Wang, C.; Clément, R. J.; Yao, Y.; Hu, E.; Ong, S. P.; Liu, P. Healable and conductive sulfur iodide for solid-state Li-S batteries. *Nature* **2024**, *627* (8003), 301−305.

(13) Pope, M. A.; Aksay, I. A. Structural Design of Cathodes for Li-S Batteries. *Adv. Energy Mater.* **2015**, *5* (16), 1500124.

(14) Xu, J.; Lawson, T.; Fan, H.; Su, D.; Wang, G. Updated Metal Compounds (MOFs, -S, -OH, -N, -C) Used as Cathode Materials for Lithium-Sulfur Batteries. *Adv. Energy Mater.* **2018**, *8* (10), 1702607.

(15) Fang, R.; Zhao, S.; Sun, Z.; Wang, W.; Cheng, H.-M.; Li, F. More Reliable Lithium-Sulfur Batteries: Status, Solutions and Prospects. *Adv. Mater.* **2017**, *29* (48), 1606823.

(16) Zhang, K.; Li, X.; Yang, Y.; Chen, Z.; Ma, L.; Zhao, Y.; Yuan, Y.; Chen, F.; Wang, X.; Xie, K.; Loh, K. P. High Loading Sulfur Cathodes by Reactive-Type Polymer Tubes for High-Performance Lithium-Sulfur Batteries. *Adv. Funct. Mater.* **2023**, *33* (11), 2212759.

(17) Yang, D.; Wang, J.; Lou, C.; Li, M.; Zhang, C.; Ramon, A.; Li, C.; Tang, M.; Henkelman, G.; Xu, M.; Li, J.; Llorca, J.; Arbiol, J.; Mitlin, D.; Zhou, G.; Cabot, A. Single-Atom Catalysts with Unsaturated Co-N_2 Active Sites Based on a C_2N 2D-Organic Framework for Efficient Sulfur Redox Reaction. *ACS Energy Lett.* **2024**, *9*, 2083.

(18) Huang, A.; Kong, L.; Zhang, B.; Liu, X.; Wang, L.; Li, L.; Xu, J. Electrochemical Restructuring Driven Catalytic Cycle of Bi-Based Heterojunctions for High-Performance Lithium-Sulfur Batteries. *ACS Nano* **2024**, *18*, 12795.
(19) Liu, D.; Shadike, Z.; Lin, R.; Qian, K.; Li, H.; Li, K.; Wang, S.; Yu, Q.; Liu, M.; Ganapathy, S.; Qin, X.; Yang, Q.-H.; Wagemaker, M.; Kang, F.; Yang, X.-Q.; Li, B. Review of Recent Development of In Situ/Operando Characterization Techniques for Lithium Battery Research. *Adv. Mater.* **2019**, *31* (28), 1806620.
(20) Lin, Q.; Liang, J.; Fang, R.; Sun, C.; Rawal, A.; Huang, J.; Yang, Q.-H.; Lv, W.; Wang, D.-W. A Lewis Acid-Lewis Base Hybridized Electrocatalyst for Roundtrip Sulfur Conversion in Lithium-Sulfur Batteries. *Adv. Energy Mater.* **2024**, *14* (21), 2400786.
(21) Lei, D.; Shi, K.; Ye, H.; Wan, Z.; Wang, Y.; Shen, L.; Li, B.; Yang, Q.-H.; Kang, F.; He, Y.-B. Progress and Perspective of Solid-State Lithium-Sulfur Batteries. *Adv. Funct. Mater.* **2018**, *28* (38), 1707570.
(22) Rosenman, A.; Markevich, E.; Salitra, G.; Aurbach, D.; Garsuch, A.; Chesneau, F. F. Review on Li-Sulfur Battery Systems: an Integral Perspective. *Adv. Energy Mater.* **2015**, *5* (16), 1500212.
(23) Li, X.-Y.; Feng, S.; Song, Y.-W.; Zhao, C.-X.; Li, Z.; Chen, Z.-X.; Cheng, Q.; Chen, X.; Zhang, X.-Q.; Li, B.-Q.; Huang, J.-Q.; Zhang, Q. Kinetic Evaluation on Lithium Polysulfide in Weakly Solvating Electrolyte toward Practical Lithium-Sulfur Batteries. *J. Am. Chem. Soc.* **2024**, *146* (21), 14754−14764.
(24) Hu, Y.; Chen, W.; Lei, T.; Jiao, Y.; Huang, J.; Hu, A.; Gong, C.; Yan, C.; Wang, X.; Xiong, J. Strategies toward High-Loading Lithium-Sulfur Battery. *Adv. Energy Mater.* **2020**, *10* (17), 2000082.
(25) Cheng, Z.; Pan, H.; Zhong, H.; Xiao, Z.; Li, X.; Wang, R. Porous Organic Polymers for Polysulfide Trapping in Lithium-Sulfur Batteries. *Adv. Funct. Mater.* **2018**, *28* (38), 1707597.
(26) Manthiram, A.; Fu, Y.; Chung, S.-H.; Zu, C.; Su, Y.-S. Rechargeable Lithium-Sulfur Batteries. *Chem. Rev.* **2014**, *114* (23), 11751−11787.
(27) Yang, Y.; Zheng, G.; Cui, Y. Nanostructured Sulfur Cathodes. *Chem. Soc. Rev.* **2013**, *42* (7), 3018−3032.
(28) Liu, F.; Wang, N.; Shi, C.; Sha, J.; Ma, L.; Liu, E.; Zhao, N. Phosphorus Doping of 3D Structural MoS_2 to Promote Catalytic Activity for Lithium-Sulfur Batteries. *Chem. Eng. J.* **2022**, *431*, 133923.
(29) Liu, J.; Wang, M.; Xu, N.; Qian, T.; Yan, C. Progress and Perspective of Organosulfur Polymers as Cathode Materials for Advanced Lithium-Sulfur Batteries. *Energy Storage Mater.* **2018**, *15*, 53−64.
(30) Liu, D.; Zhang, C.; Zhou, G.; Lv, W.; Ling, G.; Zhi, L.; Yang, Q.-H. Catalytic Effects in Lithium-Sulfur Batteries: Promoted Sulfur Transformation and Reduced Shuttle Effect. *Adv. Sci.* **2018**, *5* (1), 1700270.
(31) Seh, Z. W.; Sun, Y.; Zhang, Q.; Cui, Y. Designing High-Energy Lithium-Sulfur Batteries. *Chem. Soc. Rev.* **2016**, *45* (20), 5605−5634.
(32) Guo, D.; Zhang, X.; Liu, M.; Yu, Z.; Chen, X. a.; Yang, B.; Zhou, Z.; Wang, S. Single Mo-N_4 Atomic Sites Anchored on N-doped Carbon Nanoflowers as Sulfur Host with Multiple Immobilization and Catalytic Effects for High-Performance Lithium-Sulfur Batteries. *Adv. Funct. Mater.* **2022**, *32* (35), 2204458.
(33) Ren, J.; Zhou, Y.; Xia, L.; Zheng, Q.; Liao, J.; Long, E.; Xie, F.; Xu, C.; Lin, D. Rational Design of a Multidimensional N-doped Porous Carbon/MoS_2/CNT Nano-Architecture Hybrid for High Performance Lithium-Sulfur Batteries. *J. Mater. Chem. A* **2018**, *6* (28), 13835−13847.
(34) You, Y.; Ye, Y.; Wei, M.; Sun, W.; Tang, Q.; Zhang, J.; Chen, X.; Li, H.; Xu, J. Three-Dimensional MoS_2/rGO Foams as Efficient Sulfur Hosts for High-Performance Lithium-Sulfur Batteries. *Chem. Eng. J.* **2019**, *355*, 671−678.
(35) Zeng, S.; Li, L.; Xie, L.; Zhao, D.; Zhou, N.; Wang, N.; Chen, S. Graphene-Supported Highly Crosslinked Organosulfur Nanoparticles as Cathode Materials for High-Rate, Long-Life Lithium-Sulfur Battery. *Carbon* **2017**, *122*, 106−113.
(36) Sang, P.; Song, J.; Guo, W.; Fu, Y. Hyperbranched Organosulfur Polymer Cathode Materials for Li-S Battery. *Chem. Eng. J.* **2021**, *415*, 129043.
(37) Ma, J.; Fan, J.; Chen, S.; Yang, X.; Hui, K. N.; Zhang, H.; Bielawski, C. W.; Geng, J. Covalent Confinement of Sulfur Copolymers onto Graphene Sheets Affords Ultrastable Lithium-Sulfur Batteries with Fast Cathode Kinetics. *ACS Appl. Mater. Interfaces* **2019**, *11* (14), 13234−13243.
(38) Chang, W.; Qu, J.; Sui, Y.; Ji, Q.-Y.; Zhang, T.-T.; Zhai, X.-Z.; Jing, Y.-Q.; Yu, Z.-Z. Constructing Mesoporous Hollow Polysulfane Spheres Bonded with Short-Chain Sulfurs (S_x, $x \leq 3$) as High-Performance Sulfur Cathodes in Both Ether and Ester Electrolytes. *Energy Storage Mater.* **2020**, *27*, 426−434.
(39) Hu, X.; Shen, K.; Han, C.; Li, M.; Guo, J.; Yan, M.; Zhang, M. Rational Design of Ultrathin Mo_2C/C Nanosheets Decorated on Mesoporous Hollow Carbon Spheres as a Multifunctional Sulfur Host for Advanced Li-S Batteries. *J. Alloys Compd.* **2022**, *918*, 165667.
(40) Chen, G.; Li, Y.; Zhong, W.; Zheng, F.; Hu, J.; Ji, X.; Liu, W.; Yang, C.; Lin, Z.; Liu, M. MOFs-Derived Porous Mo_2C-C Nano-Octahedrons Enable High-Performance Lithium-Sulfur Batteries. *Energy Storage Mater.* **2020**, *25*, 547−554.
(41) Zhang, W.; Li, H.; Tao, R.; Guo, C.; Du, K.; Wang, J.; Yao, S.; Liu, X.; Li, H.; Guo, P.; Li, J.; Liang, J. In-situ Constructing Hetero-Structured Mo_2C-Mo_2N Embedded in Carbon Nanosheet as an Efficient Separator Modifier for High-Performance Lithium-Sulfur Batteries. *Chem. Eng. J.* **2023**, *475*, 146133.
(42) Fu, C.; Li, G.; Zhang, J.; Cornejo, B.; Piao, S. S.; Bozhilov, K. N.; Haddon, R. C.; Guo, J. Electrochemical Lithiation of Covalently Bonded Sulfur in Vulcanized Polyisoprene. *ACS Energy Lett.* **2016**, *1* (1), 115−120.
(43) Zhou, L.; Zhao, L.; Gao, X.; Chi, C.; Qiu, Z.; Song, Y.; Cai, T.; Liu, P.; Li, X.; Fan, Z.; Xue, Q.; Yan, Z.; Cui, Y.; Xing, W. Multiple Working Mechanisms Enabled by an Iodized Organic Salt Cathode for High Energy Density Potassium-Organic Batteries. *ACS Energy Lett.* **2023**, *8*, 5152−5160.
(44) Lv, L.-P.; Guo, C.-F.; Sun, W.; Wang, Y. Strong Surface-Bound Sulfur in Carbon Nanotube Bridged Hierarchical Mo_2C-Based MXene Nanosheets for Lithium-Sulfur Batteries. *Small* **2019**, *15* (3), 1804338.
(45) Yang, J.-L.; Cai, D.-Q.; Lin, Q.; Wang, X.-Y.; Fang, Z.-Q.; Huang, L.; Wang, Z.-J.; Hao, X.-G.; Zhao, S.-X.; Li, J.; Cao, G.-Z.; Lv, W. Regulating the Li_2S Deposition by Grain Boundaries in Metal Nitrides for Stable Lithium-Sulfur Batteries. *Nano Energy* **2022**, *91*, 106669.
(46) Du, Z.; Guo, Y.; Wang, H.; Gu, J.; Zhang, Y.; Cheng, Z.; Li, B.; Li, S.; Yang, S. High-Throughput Production of 1T MoS_2 Monolayers Based on Controllable Conversion of Mo-Based MXenes. *ACS Nano* **2021**, *15* (12), 19275−19283.
(47) Zhang, J.; Xu, G.; Zhang, Q.; Li, X.; Yang, Y.; Yang, L.; Huang, J.; Zhou, G. Mo-O-C Between MoS_2 and Graphene Toward Accelerated Polysulfide Catalytic Conversion for Advanced Lithium-Sulfur Batteries. *Adv. Sci.* **2022**, *9* (22), 2201579.
(48) Eng, A. Y. S.; Cheong, J. L.; Lee, S. S. Controlled Synthesis of Transition Metal Disulfides (MoS_2 and WS_2) on Carbon Fibers: Effects of Phase and Morphology toward Lithium-Sulfur Battery Performance. *Appl. Mater. Today* **2019**, *16*, 529−537.
(49) Song, H.; Li, T.; He, T.; Wang, Z.; Fang, D.; Wang, Y.; Li, X. L.; Zhang, D.; Hu, J.; Huang, S. Cooperative Catalytic Mo-S-Co Heterojunctions with Sulfur Vacancies for Kinetically Boosted Lithium-Sulfur Battery. *Chem. Eng. J.* **2022**, *450*, 138115.
(50) Wang, D.-Y.; Si, Y.; Guo, W.; Fu, Y. Long Cycle Life Organic Polysulfide Catholyte for Rechargeable Lithium Batteries. *Adv. Sci.* **2020**, *7* (4), 1902646.
(51) Je, S. H.; Kim, H. J.; Kim, J.; Choi, J. W.; Coskun, A. Perfluoroaryl-Elemental Sulfur S_NAr Chemistry in Covalent Triazine Frameworks with High Sulfur Contents for Lithium-Sulfur Batteries. *Adv. Funct. Mater.* **2017**, *27* (47), 1703947.

https://doi.org/10.1021/acsaem.4c02954
ACS Appl. Energy Mater. 2025, 8, 2360−2368

(52) Xu, M.; Liu, X.; Zhao, Z.; Sun, L.; Liu, L.; Guo, J.; Sha, J. Cross-Linking Cu-TCPP@CNT-OH-S as High Sulfur Loading Cathode for Li-S Batteries. *Chem. Eng. J.* **2024**, *491*, 152178.
(53) Li, H.; Chen, H.; Chen, Y.; Bai, G.; Zhang, M.; Zhuo, K.; Zhang, L. Enhancing the Bidirectional Reaction Kinetics of Polysulfides by Mott-Schottky-like Electrocatalysts with Rich Heterointerfaces. *ACS Sustainable Chem. Eng.* **2022**, *10* (16), 5092−5100.
(54) Chen, X.; Xu, Y.; Du, F.-H.; Wang, Y. Covalent Organic Framework Derived Boron/Oxygen Codoped Porous Carbon on CNTs as an Efficient Sulfur Host for Lithium-Sulfur Batteries. *Small Methods* **2019**, *3* (11), 1900338.
(55) Xu, J.; Wang, H.; He, T.; Yan, X.; Yu, J.; Bi, J.; Ye, D.; Yao, W.; Tang, Y.; Zhao, H.; Zhang, J. Chevrel Phase Mo_6S_8 Nanosheets Featuring Reversible Electrochemical Li-Ion Intercalation as Effective Dynamic-Phase Promoter for Advanced Lithium-Sulfur Batteries. *Small* **2023**, *19* (29), 2300042.
(56) Park, J.; Kim, E. T.; Kim, C.; Pyun, J.; Jang, H.-S.; Shin, J.; Choi, J. W.; Char, K.; Sung, Y.-E. The Importance of Confined Sulfur Nanodomains and Adjoining Electron Conductive Pathways in Subreaction Regimes of Li-S Batteries. *Adv. Energy Mater.* **2017**, *7* (19), 1700074.
(57) Lei, D.; Shang, W.; Zhang, X.; Li, Y.; Shi, X.; Qiao, S.; Wang, Q.; Zhang, Q.; Hao, C.; Xu, H.; Chen, G.; He, G.; Zhang, F. Competing Reduction Induced Homogeneous Oxygen Doping to Unlock MoS_2 Basal Planes for Faster Polysulfides Conversion. *J. Energy Chem.* **2022**, *73*, 26−34.
(58) Bhargav, A.; Bell, M. E.; Cui, Y.; Fu, Y. Polyphenylene Tetrasulfide as an Inherently Flexible Cathode Material for Rechargeable Lithium Batteries. *ACS Appl. Energy Mater.* **2018**, *1* (11), 5859−5864.
(59) Yan, R.; Zhao, Z.; Zhu, R.; Wu, M.; Liu, X.; Adeli, M.; Yin, B.; Cheng, C.; Li, S. Alveoli-Inspired Carbon Cathodes with Interconnected Porous Structure and Asymmetric Coordinated Vanadium Sites for Superior Li-S Batteries. *Angew. Chem., Int. Ed.* **2024**, *63*, No. e202404019.
(60) Wei, J.-Y.; Zhang, X.-Q.; Hou, L.-P.; Shi, P.; Li, B.-Q.; Xiao, Y.; Yan, C.; Yuan, H.; Huang, J.-Q. Shielding Polysulfide Intermediates by an Organosulfur-Containing Solid Electrolyte Interphase on the Lithium Anode in Lithium-Sulfur Batteries. *Adv. Mater.* **2020**, *32* (37), 2003012.
(61) Tao, X.; Wang, J.; Ying, Z.; Cai, Q.; Zheng, G.; Gan, Y.; Huang, H.; Xia, Y.; Liang, C.; Zhang, W.; Cui, Y. Strong Sulfur Binding with Conducting Magneli-Phase Ti_nO_{2n-1} Nanomaterials for Improving Lithium-Sulfur Batteries. *Nano Lett.* **2014**, *14* (9), 5288−5294.
(62) Zhao, Y.; Li, G.; Gao, Y.; Wang, D.; Huang, Q.; Wang, D. Stable Li Metal Anode by a Hybrid Lithium Polysulfidophosphate/Polymer Cross-Linking Film. *ACS Energy Lett.* **2019**, *4* (6), 1271−1278.
(63) Su, Y.-S.; Fu, Y.; Cochell, T.; Manthiram, A. A Strategic Approach to Recharging Lithium-Sulphur Batteries for Long Cycle Life. *Nat. Commun.* **2013**, *4*, 2985.
(64) Liang, X.; Hart, C.; Pang, Q.; Garsuch, A.; Weiss, T.; Nazar, L. F. A Highly Efficient Polysulfide Mediator for Lithium-Sulfur Batteries. *Nat. Commun.* **2015**, *6*, 5682.
(65) Chen, S.; Dai, F.; Gordin, M. L.; Yu, Z.; Gao, Y.; Song, J.; Wang, D. Functional Organosulfide Electrolyte Promotes an Alternate Reaction Pathway to Achieve High Performance in Lithium-Sulfur Batteries. *Angew. Chem., Int. Ed.* **2016**, *55* (13), 4231−4235.
(66) Wu, M.; Cui, Y.; Bhargav, A.; Losovyj, Y.; Siegel, A.; Agarwal, M.; Ma, Y.; Fu, Y. Organotrisulfide: A High Capacity Cathode Material for Rechargeable Lithium Batteries. *Angew. Chem., Int. Ed.* **2016**, *55* (34), 10027−10031.

https://doi.org/10.1021/acsaem.4c02954
ACS Appl. Energy Mater. 2025, 8, 2360−2368